Magazine of Civil Engineering

ISSN 2712-8172

journal homepage: http://engstroy.spbstu.ru/

Research article

UDC 624

DOI: 10.34910/MCE.134.10

Experimental study on the behavior of multilayer geosynthetic-reinforced sandy embankments

H.A. Al-Salamy, M.A. Al-Naddaf ✉ , ***R.A. Almuhanna***

The University of Kerbala, Karbala, Iraq

✉ *mahdi.a@uokerbala.edu.iq*

Keywords: geosynthetic reinforcement, laboratory model, plate loading test, sandy embankment.

Abstract. A significant number of transportation embankments fail before their design life due to poor quality of construction materials, inadequate compaction, embankment construction, and overloading. To overcome this issue, increasing the strength and rigidity of the embankment layers is necessary to lower the stresses on the sub-layers. This paper aims to advance the knowledge of using multilayer geosynthetic reinforcements to improve the performance of sandy embankments. Four laboratory model tests with reinforced and unreinforced embankment were conducted in a box of inner dimensions of 2.40(L)×1.15(W)×1.20(H) m. Local poorly graded sand (A3 soil) was used as fill material to construct a 450 mm high embankment with a 1:1 side slope resting on a 300 mm high of sandy subgrade soil. In the reinforced embankments, three layers with 150 mm vertical spacing of either geotextile, geogrid, or geocomposite (i.e., geotextile sheet over geogrid) were utilized in each model test. Several non-distractive tests, e.g., lightweight deflectometer, dynamic cone penetration, and field California bearing ratio tests, were performed during the embankment construction. In each test, two static plate loading tests were conducted to evaluate the embankment performance and the benefit of geosynthetic reinforcement. The study showed that geosynthetic reinforcement significantly decreased surface settlement and increased load-carrying capacity. The results indicate that the load-carrying capacity near the embankment side slope can be significantly increased by the inclusion of geosynthetic layers and that the magnitude of capacity increase depends greatly on the geosynthetic type. The results also demonstrate that geogrid lateral restrain and confinement were more effective alternatives to sublayer improvement than geotextile or geocomposite.

Citation: Al-Salamy, H.A., Al-Naddaf, M.A., Almuhanna, R.A. Experimental study on the behavior of multilayer geosynthetic-reinforced sandy embankments. Magazine of Civil Engineering. 2025. 18(2). Article no. 13410. DOI: 10.34910/MCE.134.10

1. Introduction

Since the highway transportation network has grown significantly in recent years, designers have begun to decrease route lengths and trip times. Geosynthetics have long been used to improve soft soil conditions for projects, such as highway embankments, seawalls, and building foundations, as well as to cover excavated and backfilled trenches. Geosynthetics, such as geotextiles (GTs) and geogrids (GGs), have been widely employed in geotechnical engineering for a variety of applications. Reinforcement, filtration, separation, drainage, protection, and fluid barriers are all common uses for geosynthetics [1].

Roadways were built to pass through locations with a variety of tough terrains, necessitating the development of constructions, such as steep embankments. Controlling the stability and settling of embankments under various loading circumstances has always been a difficult task for designers [2]. In general, ground improvement techniques, such as vibro stone columns, are utilized to reinforced embankment bases in soft soils. The use of geosynthetic reinforcements to improve the stability of

embankments has become popular recently. Improving the engineering qualities of soil by using reinforcement layers is a valuable option. The beneficial effect of geosynthetic material as reinforcement is largely determined by the form in which it is applied. When the same geosynthetic material is utilized in planar layers (e.g., geogrids or geotextiles), three dimensional (e.g., geocells), or discrete fibers, they would yield distinct strength gains in different forms. This disparity in strengthening the soil is mostly due to differences in failure mechanisms in soil reinforced with geosynthetic material in various forms. Friction and interlocking between soil and reinforcement improve the strength of horizontal geosynthetic layers, whereas friction and coiling around soil particles improve the strength of randomly oriented fibers [3].

Much research has been carried out to understand the beneficial effects of planar form of reinforcement in sand using geosynthetic layers, such as those discussed in [4–7]. Several studies are also available on the use of randomly oriented discrete geosynthetic fibers to reinforce sand, such as those discussed in [8–14]. Some studies are also available on sand reinforced with 3D inclusions made of galvanized iron sheet and hard plastic sheet [15]. In addition, the concept of cellular geosynthetic reinforcement is studied in several previous studies [16–19].

In the past two decades, some laboratory and field research projects have been conducted to investigate the performance of the geogrid-supported embankments on soft subgrades. Geocomposite (GC) reinforcements are now successfully utilized for different geotechnical structures like sloped embankment. A review on the literature suggests that geosynthetics have been abundantly used in road and railway projects during the recent years. Most of these projects are based on placing geosynthetic layers as reinforcement in superstructure layers of roads and railways [2]. An extensive range of studies have been carried out on geogrid inclusion under foundation to evaluate the bearing capacity of geogrid-reinforced soil using laboratory model tests. On the other hand, geotextile provides separation and filtration functions, preventing the intermixing of granular layers and the ingress of fines. Their use ensures an improved performance and design life of the materials layers in several application [20].

The present study aims to find the effect of geotextile, geogrid, and geocomposite reinforcement in sandy soil embankment and evaluate their behavior in comparison with unreinforced (UR) case. In addition, evaluating the reinforcement benefits in sliding control of embankment slopes and decreasing the surface settlement under loading are of great interest.

2. Methods and Materials

2.1. Physical and Chemical Properties of Embankment Soil

As illustrated in Fig. 1(a), the soil was collected from the site of Karbala Airport. It was classified as (A-3) soil and poorly graded sand (SP) according to the American Association of State Highway and Transportation Officials (AASHTO M145-91, 2012) and the American Society for Testing and Materials (ASTM D 2487), respectively. Fig. 1(b) depicts the grain size distribution of this soil. The main tests were done to determine the basic characteristics of soil that will be utilized in the physical model tests. These tests are the modified Proctor test (ASTM D 1557) to obtain the maximum dry density of the soil and the optimum moisture content, particle size distribution (ASTM D2487) to classify the soil, specific gravity (ASTM D854), and California bearing ratio (CBR) test (ASTM D1883). The parameters of the sand utilized in the investigation are listed in Table 1. As a subgrade and embankment material, sand is employed.

(a)

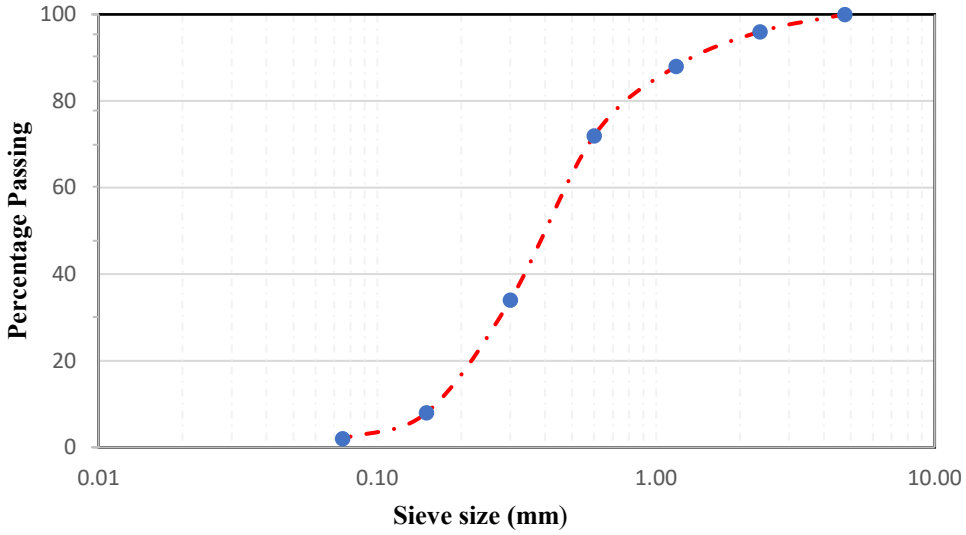

(b)

Figure 1. (a) Soil of Kerbala Airport; (b) Grain Size Distribution of Soil.

Table 1. Physical and Chemical Characteristics of Sandy Soil.

Property	Tests Result	Specification
AASHTO Classification	A-3	AASHTO M145
USCS Classification	Poorly Graded Sand (SP)	ASTM D 2487
Max. Dry Unit Weight (g/cm^3)	1.925	ASTM D 1557
CBR at 95 %	22 %	
OMC	11 %	ASTM D 1557
D10	0.14	ASTM D 2487
D30	0.3	ASTM D 2487
D60	0.6	ASTM D 2487
Specific Gravity	2.57	ASTM D 854
Uniformity Coefficient (Cu)	4.28	ASTM D 2487
Curvature Coefficient (Cc)	1.07	ASTM D 2487
Chemical Characteristics		
SO3	9.9	B.S Part 3
Gypsum	21.3	B.S Part 3
PH	7.9	B.S Part 3
CL	79.9	B.S Part 3

2.2. Geosynthetic Reinforcement

Biaxial geogrid of 30 mm aperture size is used in this study. The properties of the geogrid used are shown in Table 2. Polypropylene non-woven geotextile (A401) having mass per unit area of 300 g/m^2 is used in the present study. Table 3 shows the various properties of geotextile.

Table 2. Specification of Geogrid.

Property	Type or Value
Standard Color	Black
Polymer Type	Polypropylene
Aperture Size (mm)	30
Weight (g/m^2)	370
Peak Tensile Strength (MPa)	30
Beak Extension (kN/m)	L=15, W=11

Table 3. Properties of Non-Woven Polypropylene Geotextile.

Particulars	Test Method	Value
Tensile Strength (CD) (KN/m)	EN ISO 10319	17
Tensile Strength (MD) (KN/m)	EN ISO 10319	11.2
CBR Puncture (N)	EN ISO 12236	2380
Permeability ($10^3 ms^{-1}$)	EN ISO 111058	55
Tensile Elongation (%)	EN ISO 10319	55/66
Mass / Unit Area (g/m^2)	EN ISO 10319	300
Thickness (mm) under 2Kpa	EN ISO 9863-1	2.8
Color		White

For the application of load on the embankment, a loading chamber with specified dimensions must be modelled. After proper scaling, four series of embankments should also be modelled.

2.3. Subgrade Preparation

The embankment is built with a height of 0.45 m over a 0.30 m thick subgrade in the loading chamber, taking into account the height of the loading chamber. Subgrade material was poor graded (PW) sand with a uniformity coefficient (Cu) of 4.2857 and a curvature coefficient (Cc) of 1.0714. The dirt was compacted with optimum wetness in 15 cm layers using suitable roller weights up to a height of 0.30 m from the chamber's foundation to create the subgrade.

2.4. Embankment Modelling

In this study, a 0.45 m height embankment with a side slope of 1:1 is selected as the reference embankment. The scaling law was applied on the aforementioned embankment with a scale of 1:4 for the laboratory test programmer. A side slope of 1:1 is selected for laboratory model. The poor graded (PW) sand with uniformity coefficient (Cu) of 4.2857 and curvature coefficient (Cc) of 1.0714 was adopted as the embankment material. The maximum dry density of this soil has been obtained equal to 1.925 g/cm^3 in the optimum moisture 11 %. The dimensions of the laboratory model are given in Table 4. Fig. 2 shows the schematic diagram of the model embankment.

Table 4. The Dimensions of the Laboratory Model.

Parameter	Laboratory Embankment
Embankment Length (m)	2.41
Embankment Height (m)	0.45
Subgrade Height (m)	0.30
Width of Bed Side (m)	0.30

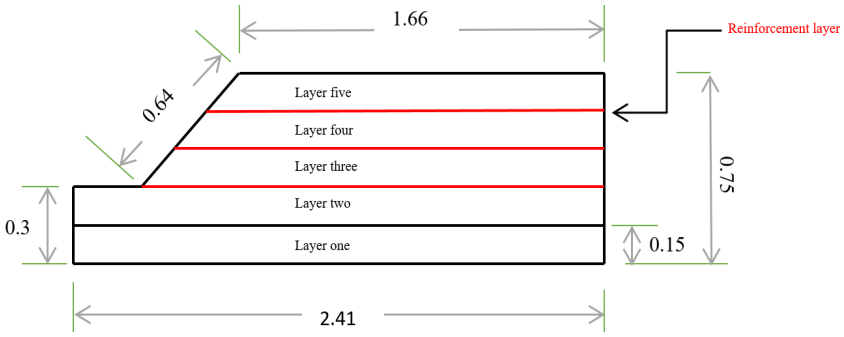

Figure 2. The Schematic Diagram of the Model Embankment.

2.5. Model Preparation and Test Procedure

A steel box with dimensions of length = 2.4 m, height = 1.2 m, width = 1.2 m was utilized to approximate in-situ subgrade conditions. The steel box's purpose was to represent the subgrade and embankment layers so that compaction and other tests could be performed. Four series of models were constructed one without reinforcement and three with reinforcement with geogrid, with geotextile and with a composite of them. Each model was built to represent a cross-section of a railway. The model contains two layers to represent the subgrade with a height of 15 cm for each layer and contains three layers to

represent the embankment with a height of 15 cm for each layer. Three layers of reinforcement were placed between the layers of the embankments and between the second layer of the subgrade and the first layer of the embankment.

The preparation of the model involves several steps to improve the density of the subgrade and embankment samples, each layer was compacted. The compacted effort was achieved with 8 passes for subgrade and 10 passes for embankments on each layer using a compaction unit. During the creation of the model layers, Table 5 illustrated a number of field tests that were carried out for each of the model layers as plate loading test (PLT), CBR, lightweight deflectometer (LWD), sand replacement method (SRM), and dynamic cone penetration (DCP) tests as shown in Fig. 3.

Table 5. Type of Layer Tests.

No. of Layer	Description	Type and Number of Tests			
1	Subgrade	3 SRM			
2	Subgrade	3 SRM	3 LWD	3 DCP	
3	Embankment	3 SRM	3 LWD	3 DCP	
4	Embankment	3 SRM	3 LWD	3 DCP	3 CBR
5	Embankment	3 SRM	3 LWD	3 DCP	2 PLT

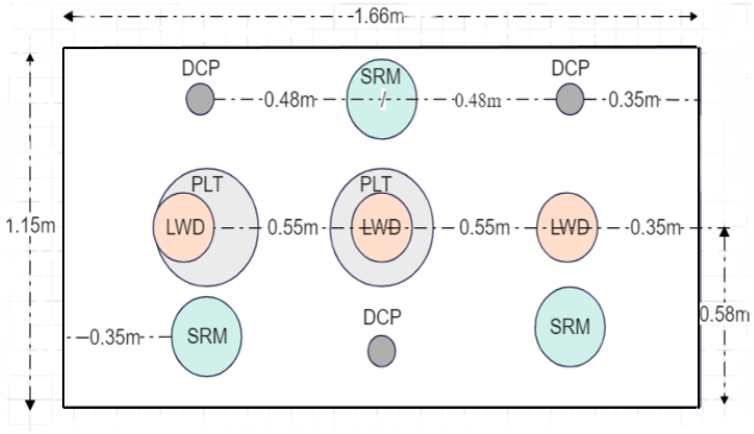

(a)

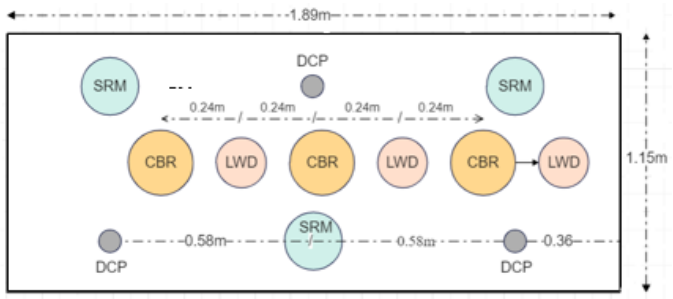

(b)

Figure 3. Location of Field Tests: (a) Layer 4 ;(b) Layer 5.

3. Results and Discussion

3.1. Results of SRM Test

As a quality control test of the construction process for all model tests, SRM test was performed in this experimental work in accordance with ASTM D155. The compaction efforts were achieved by applying different number of passes using a vibratory compactor on the top of each layer of the subgrade and the embankment in all model tests. Three SRM test points were selected and performed on the top of each layer of subgrade and embankment, and then an average value is calculated and reported. Table 5 summarizes the results of the moisture content, dry density, and relative compaction of the subgrade and the embankment layers. The results show that the average relative compaction results of subgrade soil are in the range from 88 to 92 %, and those of the embankment ranged from 91 to 92 %. This indicates an acceptable level of quality and consistency for all model tests.

Table 5. Summarizes the Results of SRM and the Relative Compaction.

Model Types			No. of Passes	Unreinforced Test (URT)	Geotextile-Reinforced Test (RT-GT)	Geogrid-Reinforced Test (RT-GG)	Geocomposite-Reinforced Test (RT-GC)
				Average of Three Test Points			
Subgrade	Layer 1	W.C%	8	11.33	10.31	10.42	8.35
		Dry Density		1.68	1.76	1.77	1.81
		R.C%		87	91	92	94
	Layer 2	W.C%	8	9.94	11.7	11.32	10.2
		Dry Density		1.71	1.79	1.77	1.74
		R.C%		89	93	92	90
	Avg.	W.C%		10.64	10.87	10.87	10.1
		Dry Density		1.70	1.77	1.77	1.78
		R.C%		88	92	92	92
Embankment	Layer 3	W.C%	10	9.93	10.09	8.62	10.29
		Dry Density		1.77	1.76	1.79	1.72
		R.C%		92	91	93	89
	Layer 4	W.C%	10	10.26	12.11	10.29	10.15
		Dry Density		1.75	1.74	1.75	1.75
		R.C%		91	91	91	91
	Layer 5	W.C%	10	8.41	9.477	8.78	9.36
		Dry Density		1.72	1.81	1.76	1.78
		R.C%		90	94	92	93
	Avg.	W.C%		9.53	9.23	9.23	9.93
		Dry Density		1.74	1.77	1.77	1.75
		R.C%		91	92	92	91

3.2. Results of DCP Test

Depending on the obtained data of the DCP test, the in-site CBR values for each subgrade layer (i.e., Layers 1 and 2) and embankment layer (i.e., Layers 3, 4, and 5) were estimated by using the empirical relation shown in Eq. 1 (21).

$$CBR = \frac{292}{DCPI^{1.12}}. \quad (1)$$

Table 6 presents the CBR results for the unreinforced and geosynthetic-reinforced (i.e., geotextile-, geogrid-, and geocomposite-reinforced) embankments Eq. 4-1.

Furthermore, the elastic modulus (E) was determined based on the obtained data of the DCP test and the CBR value using Eq. 4-2 (22).

$$E = 17.6 * CBR^{0.64}. \quad (2)$$

In summary, and even though there is some variation in the obtained results for the CBR values for all model test, the embankment layer constructed with geosynthetic reinforcement shows a higher value of CBR than the unreinforced model except for layer five. When comparing the geotextile-reinforced embankment to the geogrid-reinforced embankment, the CBR values have shown that the geotextile-reinforced model has a higher value than the geogrid-reinforced one, which agrees with the results of M. M. Singh et al. [22]; and that the geocomposite-reinforced model has the most significant value as shown in Fig. 4. This is related to the type of reinforcement and the condition of the DCP test. The DCP cone needs higher energy to penetrate through the geotextilelayer within the soil mass in both RT-GT and RT-GC, however, less energy is required in the RT-GG due to the existence of its aperture opening.

Table 6. Result of CBR Value and Value of E from DCP Test.

No. of Layer	No. of Point	The Value of CBR (%)			
		URT	RT-GT	RT-GG	RT-GC
1	1	5.40	4.10	4.45	5.24
	2	3.84	4.406	4.26	4.71
	3	3.92	4.82	4.21	4.76
	Average	4.39	4.44	4.31	4.90
2	1	3.73	2.95	2.80	4.24
	2	2.70	3.30	2.76	3.28
	3	2.69	3.66	3.10	3.24
	Average	3.04	3.30	2.89	3.59
3	1	3.56	3.12	3.17	3.66
	2	3.50	3.50	2.52	3.88
	3	3.68	3.26	2.97	4.13
	Average	3.58	3.29	2.89	3.89
4	1	3.74	3.77	3.49	4.14
	2	2.68	3.67	3.45	3.19
	3	5.23	4.66	4.09	3.59
	Average	3.88	4.03	3.67	3.64
5	1	6.73	3.72	3.15	3.38
	2	4.98	3.47	3.30	4.87
	3	6.97	3.40	3.98	3.37
	Average	6.23	3.53	3.48	3.87

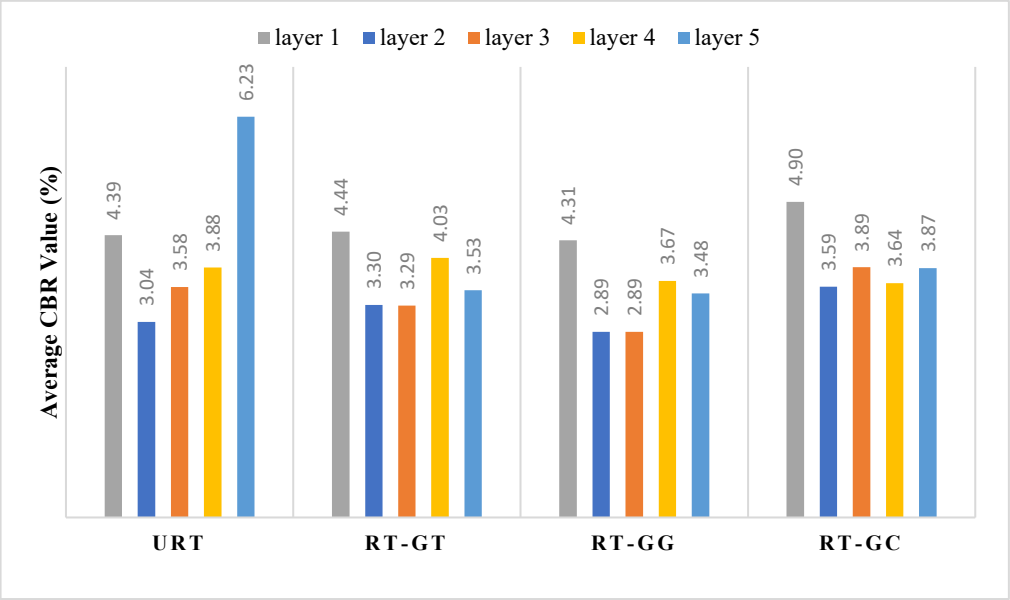

(a)

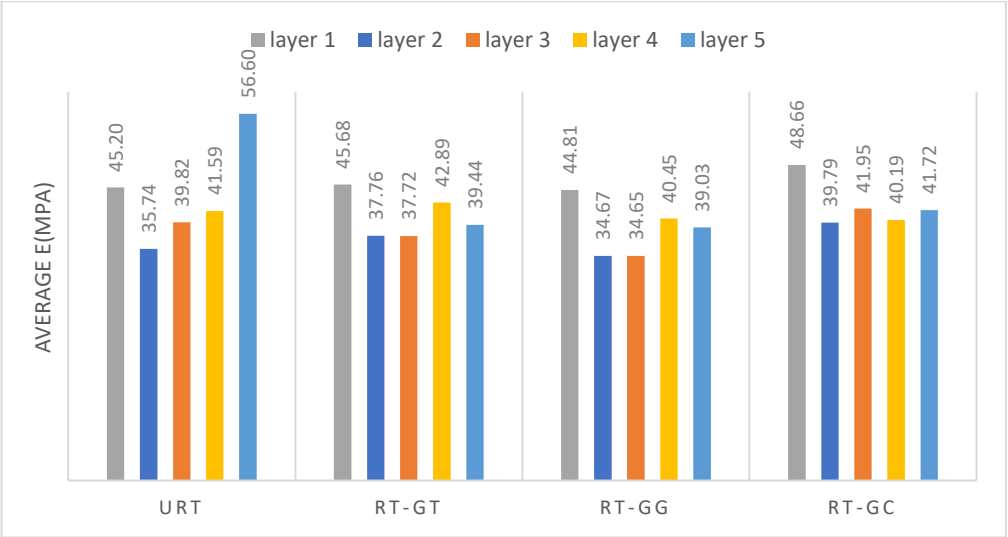

(b)

Figure 4. (a) Value of CBR from DCP Test, (b) Value of E from DCP Test.

3.3. Results of LWD Test

Three LWD tests were performed on the top of the Layers 2, 3, 4, and 5 in all physical models; these tests were distributed at three different locations on the top of each layer in the unreinforced and geosynthetic-reinforced models. Table 7 shows the results of these LWD tests. The dynamic modulus values (E_{vd}) ranged from 13.8 to 14.5 MPa for all subgrade soil in all model tests, which show a consistent construction. In addition, the E_{vd} values were from 14.3 to 15.0 MPa along embankment layers of the unreinforced model. Lower values were obtained in the geotextile-reinforced and geocomposite-reinforced model tests; the E_{vd} values ranged from 8.94 to 11.1 MPa, and from 9.8 to 12.6 MPa, respectively for RT-GT and RT-GC. However, much higher dynamic modulus was obtained for the RT-GG (i.e., 15.5–25.1 MPa).

In addition, Fig. 5 shows the value of dynamic modulus graphically for each layer in all model tests. The results indicate that E_{vd} slightly increased for the unreinforced embankment layers due to the accumulative compaction efforts on each layer, while its gradually decreases for the geotextile and geocomposite models from the third to the fifth layer. This is due to the use of geotextile in these two cases, which allowed the soil to move easily over the geotextile layer and decreased the frictional resistance between the layers. On the other hand, it was observed, in the case of geogrid reinforcement, the dynamic modulus significantly increased as the embankment layer increased. This is due to a better interlocking action and confinement between the embankment layers provided by the geogrid reinforcement layers.

Table 7. Result of Modules from LWD Test.

No.of Layer	No. of Point	Tests			
		URT	RT-GT	RT-GG	RT-GC
		E_{vd} (MPa)	E_{vd} (MPa)	E_{vd} (MPa)	E_{vd} (MPa)
2	1	14.00	14.20	14.20	13.50
	2	15.37	14.90	15.36	14.98
	3	13.68	13.80	13.79	12.90
	Average	14.35	14.30	14.45	13.79
3	1	12.90	11.56	17.25	13.26
	2	15.60	11.70	15.26	11.62
	3	14.30	10.20	14.04	12.84
	Average	14.27	11.15	15.52	12.57
4	1	14.90	11.34	14.27	10.73
	2	15.00	10.72	22.70	8.96
	3	14.30	10.23	29.11	8.97

No.of Layer	No. of Point	Tests			
		URT	RT-GT	RT-GG	RT-GC
		E_{vd} (MPa)	E_{vd} (MPa)	E_{vd} (MPa)	E_{vd} (MPa)
	Average	14.73	10.76	22.03	9.55
5	1	15.13	8.33	18.50	11.14
	2	15.16	9.00	25.80	9.57
	3	14.70	9.50	31.08	8.85
	Average	15.00	8.94	25.13	9.85

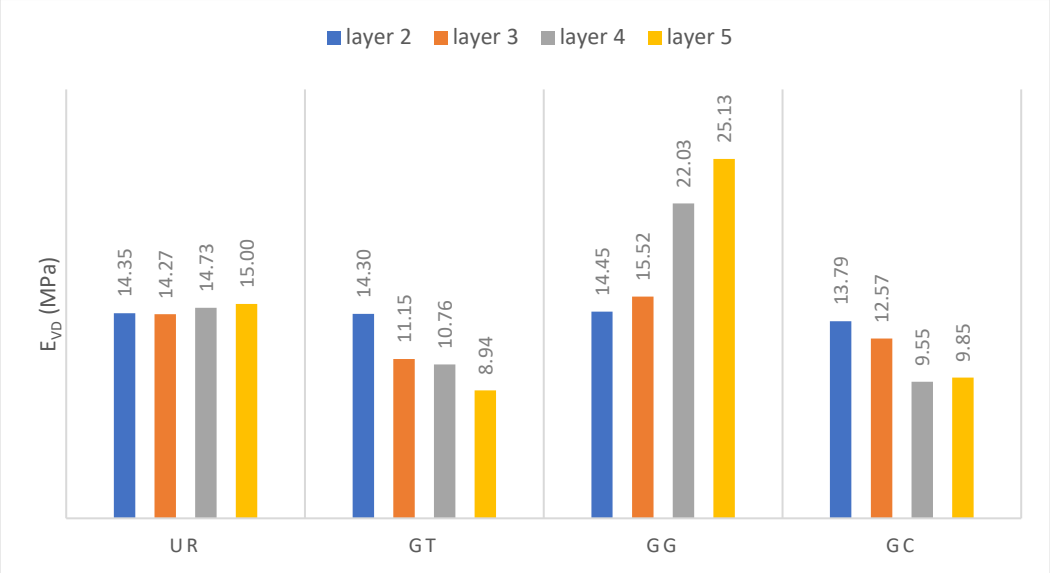

Figure 5. Value of Dynamic Modulus (E_{vd}) from LWD Test.

3.4. Results of CBR Test

The CBR test was used to determine the field CBR value of the sandy soils. There were twelve CBR tests completed during the experimental study period (i.e., three for each model test) including the geogrid-reinforced model test, but unfortunately, the data logger software did not function appropriately and the data was lost. The other nine tests were performed as follows; three tests were performed in the unreinforced model and the remaining six tests were conducted in the geotextile- and geocomposite-reinforced models. Table 8 and Fig. 6 present the results for these models, which shows that the average CBR value varies from 6.78 % for the unreinforced embankment and from 13.56 % and 14.35 % for the geotextile- and geocomposite-reinforced embankments, respectively. The increase in the CBR values for the geotextile and geocomposite model tests can be related to bearing zone underneath the CBR piston, and the tension membrane effect of the geosynthetic reinforcement.

Table 8. The Result of the CBR Field Test.

Model Name	No. of Point	CBR %
Unreinforced test (URT)	1	8.41
	2	5.80
	3	6.09
	Average	6.76
Reinforced with geotextile (RT-GT)	1	17.25
	2	11.74
	3	11.67
	Average	13.56
Reinforced with composite (RT-GG)	1	14.50
	2	14.21
	3	13.92
	Average	14.35

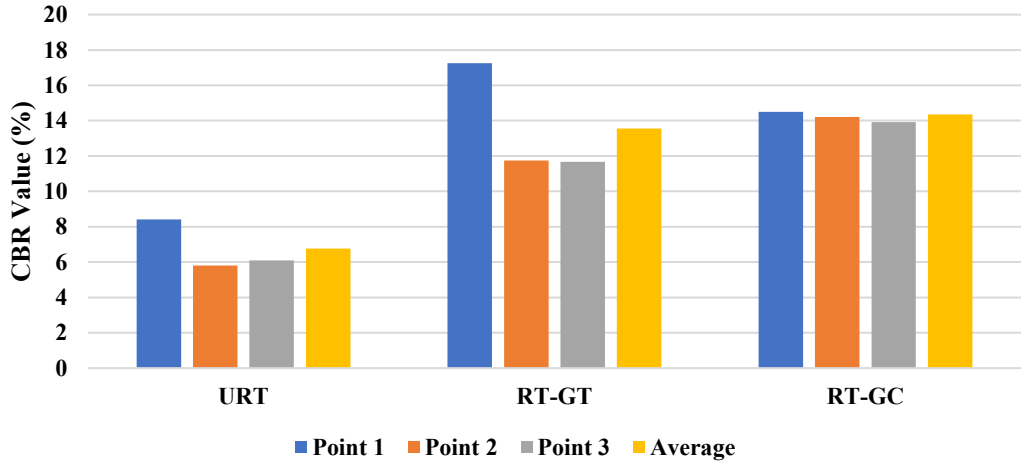

Figure 6. Comparison the Results of CBR Value for Different Models.
Point 1: it is the point near the wall of the box.
Point 2: it is the point in the center of layer four.
Point 3: it is the point near the edge of the slope.

A significant difference was observed between field CBR values and CBR values acquired from DCP test data as shown in Fig. 7. This figure shows that the value of CBR is approximately various from 3.88 % to 6.76 % in the unreinforced model, while it was changed from 4.03 % to 13.56 % in the geotextile-reinforced model and from 3.64 % to 14.35 % in the geocomposite-reinforced model. Keeping in mind that the CBR calculated from the DCP test are based on an empirical equation that have not adequately represented the CBR value, while those calculated from the field CBR test are much closer to the laboratory CBR value of the soil.

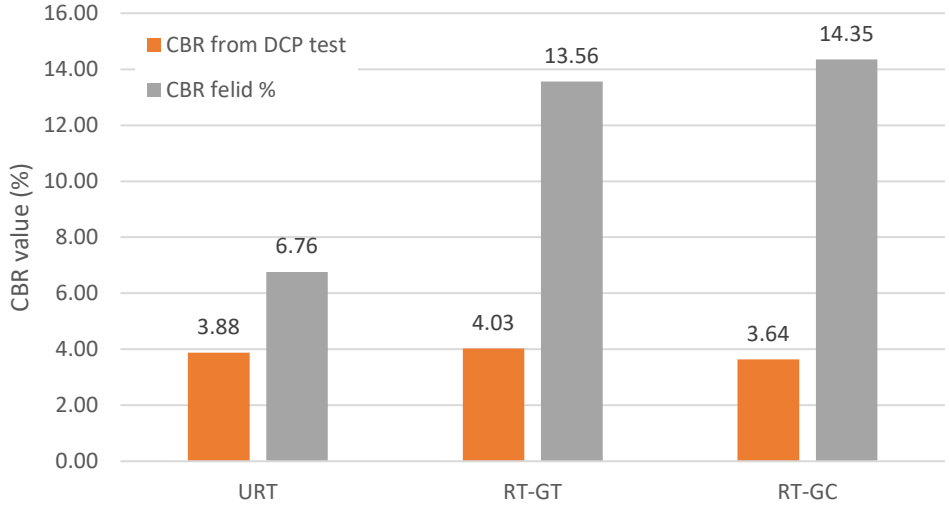

Figure 7. Compares the Value of CBR in Field and the CBR Value from DCP Test.

3.5. Results of PLT

Static PLTs were performed in all model tests to assess the load carrying capacity and calculate the subgrade modulus for the unreinforced and geosynthetic-reinforced embankments, as well as evaluating the benefits of using different geosynthetic products. Two points were selected to perform the PLT in each model test, one at the center of the embankment width (i.e., this represents a point under the railway track for the embankment configuration/dimension chosen in this study) and the other point near the slope to assess the benefit of geosynthetic reinforcement in stabilizing the slope.

3.5.1. Load-Settlement Results

Fig. 8 presents the load (stress)-settlement curve for the PLTs at the mid-point of all model tests. As shown in this figure, the unreinforced embankment has the highest settlement as compared to the

geosynthetic-reinforced model tests. However, the RT-GG has the lowest settlement or the highest bearing capacity, followed by the RT-GT and the RT-GC, respectively. For comparisons, at an applied vertical stress of 1000 kPa, the soil surface settlements under the plate were 8.0, 6.5, 5.3, and 1.7 mm for the URT, RT-GC, RT-GT, and RT-GG, respectively. This corresponding to a reduction in the surface settlement of 19, 34, and 79 % for the geocomposite, geotextile, and geogrid reinforcement, respectively, as compared to the unreinforced condition. Similarly, for the PLTs at the edge-point, the RT-GG performed the best followed by the RT-GT and RT-GC as compared to the URT as shown in Fig. 9. This can be attributed to the shearing resistance and the tensioned membrane effects of the geosynthetic under the plate.

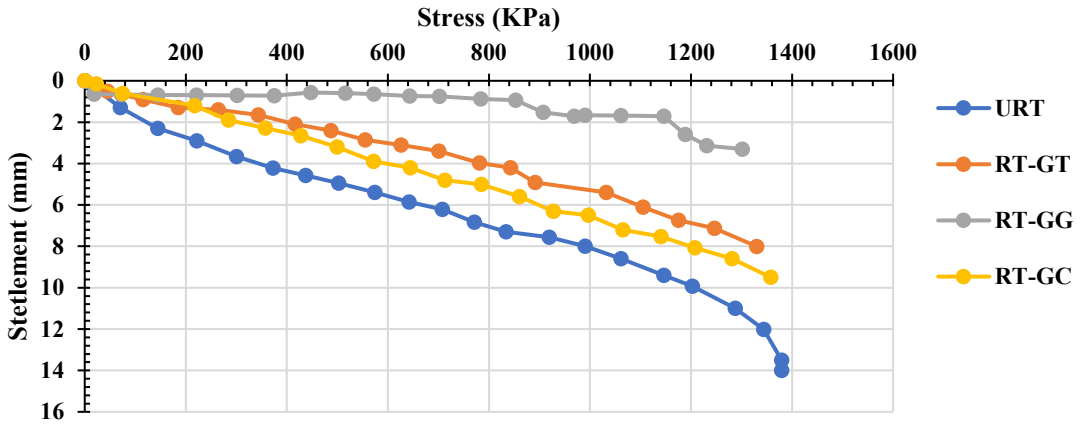

Figure 8. Stress-Settlement Curves of the PLT in URT, RT-GT, RT-GG, and RT-GC at the Embankment Mid-Point.

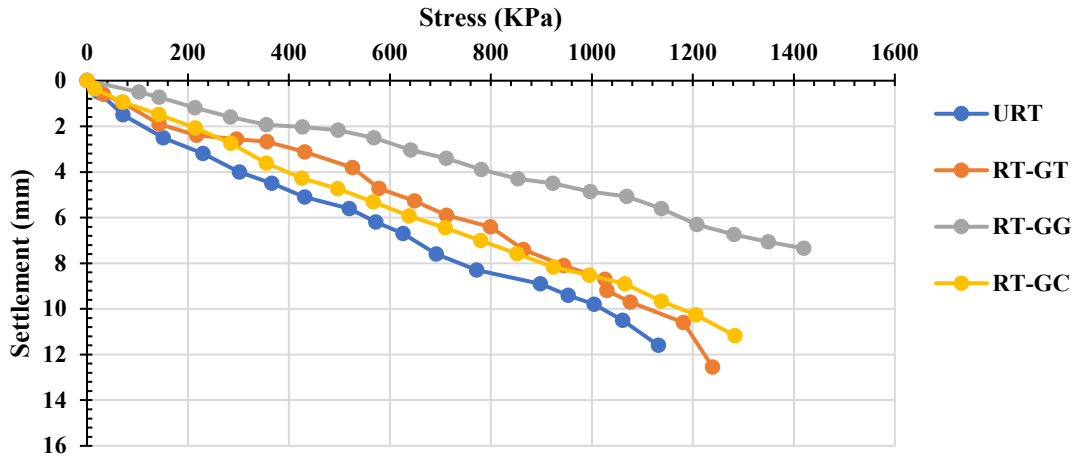

Figure 9. Stress-Settlement Curves of the PLT in URT, RT-GT, RT-GG, and RT-GC at the Embankment Edge-Point.

The subgrade reaction modulus (K_s) and E for all model tests are listed in Table 9. It was noted that the value of K_s calculated from actual curve in the PLT at the mid-point equal to 53.08 kPa/mm for unreinforced model, which is in agreement with (24) finding, while the K_s valve was equal to 111.29, 115.00, and 173.33 kPa/mm for the models reinforced with geotextile, geogrid, and geocomposite, respectively. Whereas the K_s value obtained from the corrected curve varied from 38.25 kPa/mm for unreinforced model to 181.58, 575.00, and 73.33 kPa/mm for the models reinforced with geotextile, geogrid, and geocomposite, respectively. The value of E changed from 17.59 MPa in unreinforced model to 44.17, 38.58, and 33.43 MPa in the models reinforced with geotextile, geogrid, and geocomposite, respectively. On the other hand, it was noted in Table 9 for the results of the PLTs at the edge-point that there is an apparent change in the test results when compared with the middle point test. Values changed significantly due to the proximity of the test point to the edge of the embankment slope.

Table 9. The Result of PLT.

Model Type	Test Location					
	Mid-Point			Edge-Point		
	K_s (kPa/mm) of Actual Curve	K_s (kPa/mm) of Corrected Curve	E (MPa)	K_s (kPa/mm) from Actual Curve	K_s (kPa/mm) of Corrected Curve	E (MPa)
UR	53.08	115	17.59	46.31	98.57	19.52
GT	111.29	181.58	44.16	71.88	115.00	25.04
GG	102	575.00	84.56	191.67	191.67	41.43
GC	173.33	173.33	33.43	75.00	75.00	24.10

3.5.2. Failure Mechanism of the Physical Models

The sliding surface covers more than half of the embankment in the unreinforced model. The sliding surface gradually moves towards the higher part of the reinforced region and at the interface between reinforcing layers and soil as the geosynthetic layers are positioned in the embankment. Failure is identified as cracks only in the upper half when reinforced with layers of geosynthetic as clear in RT-GT, due to the presence of the geotextile reinforcement layers, which have the property of separating between the layers and it provides the process of sliding between the layers. While the lines of failure were clear along the layers in the URT. However, the line of failure slights appeared lowest in RT-GG, which may be the result of the skin friction and interlocking between geogrid and soil particles. Fig. 10 depicts the failure pattern of geosynthetics-reinforced laboratory embankments.

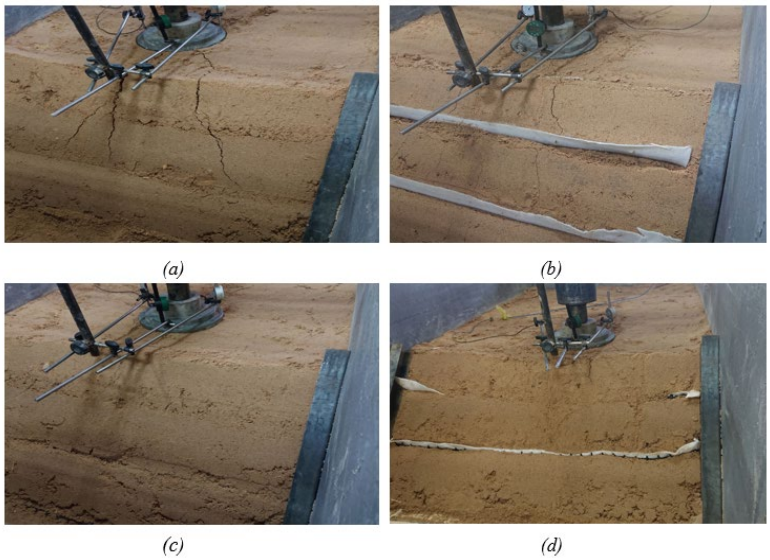

Figure 10. Failure Mechanism in the Embankments: (a) URT, (b) RT-GT, (c) RT-GG, and (d) RT-GC.

4. Conclusions

Depending on the results of the experimental that were obtained, the following conclusions are summarized:

1. The results of SRM show that the average relative compaction results of subgrade soil were in the range from 88 to 92 %, and those of the embankment ranged from 91 to 92 %, which led to an acceptable level of quality and consistency for all model tests.
2. Even though there is some variation in the obtained results for the CBR values for all model test, the embankment layer constructed with geosynthetic reinforcement show a higher value of CBR than the unreinforced model except for layer five. The CBR values have shown that the RT-GT model has a higher value than the RT-GG one; and that the RT-GC model has the most significant value.

3. The E_{vd} ranged from 13.8 to 14.5 MPa for all subgrade soil in all model tests, which show a consistent construction. In addition, the E_{vd} were from 14.3 to 15.0 MPa along the embankment layers of the unreinforced model test. Lower values were obtained in the geotextile and geogrid model tests; the E_{vd} ranged from 8.94 to 11.1 MPa, and 9.8 to 12.6 MPa for RT-GT and RT-GC, respectively. However, a much higher dynamic modulus was obtained for RT-GG (i.e., 15.5–25.1 MPa).

4. In addition, the results indicate that E_{vd} slightly increased for the unreinforced embankment layers due to the accumulative compaction efforts on each layer, while it gradually decreases for the RT-GT and RT-GC models from the third to the fifth layer. On the other hand, it was observed, in RT-GG, the dynamic modulus significantly increased as the embankment layer increased.

5. The results for the CBR of these models showed that the average CBR value varies from 6.78 % for URT and from 13.56 % and 14.35 % for the RT-GT and RT-GC, respectively. The increase in the CBR values for the geotextile and geocomposite model tests can be related to the bearing zone underneath the CBR piston and the tension membrane effect of the geosynthetic reinforcement.

6. In the PLT, the results showed that RT-GG gave the best values for K_s and E as compared to other models. As well as there is less vertical settlement in it compared with the unreinforced model.

7. The result showed that the unreinforced embankment has the highest settlement as compared to the geosynthetic reinforced model tests. However, RT-GG has the lowest settlement or the highest bearing capacity, followed by RT-GT and RT-GC, respectively. Similarly, for the PLTs at the edge point, RT-GG performed the best followed by RT-GT and RT-GC as compared to URT. This can be attributed to the shearing resistance and the tensioned membrane effects of the geosynthetic under the plate.

References

1. Shukla, S.K. Handbook of Geosynthetic Engineering: Geosynthetics and their applications. ICE. London. 2012. 409 p. DOI: 10.1680/hge.41752
2. Esmaeili, M., Naderi, B., Neyestanaki, H.K., Khodaverdian, A. Investigating the effect of geogrid on stabilization of high railway embankments. Soils and Foundations. 2018. 58(2). Pp. 319–332. DOI: 10.1016/j.sandf.2018.02.005
3. Chandrasekaran, B., Broms, B.B., Wong K.S. Strength of fabric reinforced sand under axisymmetric loading. Geotextiles and Geomembranes. 1989. 8(4). Pp. 293–310. DOI: 10.1016/0266-1144(89)90013-7
4. Krishnaswamy, N.R., Isaac, N.T. Liquefaction potential of reinforced sand. Geotextiles and Geomembranes. 1994. 13(1). Pp. 23–41.
5. Haeri, S.M., Noorzad, R., Oskoorouchi, A.M. Effect of geotextile reinforcement on the mechanical behavior of sand. Geotextiles and Geomembranes. 2000. 18(6). Pp. 385–402. DOI: 10.1016/S0266-1144(00)00005-4
6. Rao, V.G., Dutta, R.K., Ujwala, D. Strength characteristics of sand reinforced with coir fibers and coir geotextiles. Electronic Journal Of Geotechnical Engineering. 2005. 10 G.
7. Gray, D.H., Ohashi, H. Mechanics of fiber reinforcement in sand. Journal of Geotechnical Engineering. 1983. 1109(3). Pp. 335–353.
8. Gray, D.H., Al-Refeai, T. Behavior of Fabric-Versus Fiber-Reinforced Sand. Journal of Geotechnical Engineering. 1986. 112(8). Pp. 804–820. DOI: 10.1061/(ASCE)0733-9410(1986)112:8(804)
9. Al-Refeai, T.O. Behavior of granular soils reinforced with discrete randomly oriented inclusions. Geotextiles and Geomembranes. 1991. 10(4). Pp. 319–333. DOI: 10.1016/0266-1144(91)90009-L
10. Ranjan, G., Vasan, R.M., Charan, H.D. Behaviour of plastic-fibre-reinforced sand. Geotextiles and Geomembranes. 1994. 13(8). Pp. 555–565. DOI: 10.1016/0266-1144(94)90019-1
11. Kaniraj, S.R., Gayathri, V. Geotechnical behavior of fly ash mixed with randomly oriented fiber inclusions. Geotextiles and Geomembranes. 2003. 21(3). Pp. 123–149. DOI: 10.1016/S0266-1144(03)00005-0
12. Yetimoglu, T., Salbas, O. A study on shear strength of sands reinforced with randomly distributed discrete fibers. Geotextiles and Geomembranes. 2003. 21(2). Pp. 103–110. DOI: 10.1016/S0266-1144(03)00003-7
13. Park, T., Tan, S.A. Enhanced performance of reinforced soil walls by the inclusion of short fiber. Geotextiles and Geomembranes. 2005. 23(4). Pp. 348–361. DOI: 10.1016/j.geotexmem.2004.12.002
14. Zhang, M.X., Javadi, A.A., Min, X. Triaxial tests of sand reinforced with 3D inclusions. Geotextiles and Geomembranes. 2006. 24(4). Pp. 201–209. DOI: 10.1016/j.geotexmem.2006.03.004
15. Bathurst, R.J., Karpurapu, R. Large-Scale Triaxial Compression Testing of Geocell-Reinforced Granular Soils. Geotechnical Testing Journal. 1993. 16(3). Pp. 296–303. DOI: 10.1520/GTJ10050J
16. Rajagopal, K., Krishnaswamy, N.R., Latha, G.M. Behaviour of sand confined with single and multiple geocells. 1999. 17(3). DOI: 10.1016/S0266-1144(98)00034-X.
17. Madhavi Latha, G. Investigations on the behaviour of geocell supported embankments. Ph.D. Thesis. Indian Institute of Technology Madras. Chenai, 2000.
18. Dash, S.K., Rajagopal, K., Krishnaswamy, N.R. Performance of different geosynthetic reinforcement materials in sand foundations. Geosynthetics International. 2004. 11(1). Pp. 35–42. DOI: 10.1680/gein.2004.11.1.35

19. Lawson, C.R. Subgrade Stabilisation with Geotextiles. Geosynthetics International. 1995. 2(4). Pp. 741–763. DOI: 10.1680/gein.2.0034
20. Webster, S.L., Grau, R.H., Williams, T.P. Description and Application of Dual Mass Dynamic Cone Penetrometer. US Army Corps of Engineering. Washington DC, 1992. 52 p.
21. Powell, W.D., Potter, J.F., Mayhew, H.C., Nunn, M.E. The Structural Design of Bituminous Roads. TRRL Report LR 1132. Transport and Road Research Laboratory, 1984. 62 p.
22. Singh, M., Trivedi, A., Shukla, S.K. Influence of geosynthetic reinforcement on unpaved roads based on CBR, and static and dynamic cone penetration tests. International Journal of Geosynthetics and Ground Engineering. 2020. 6(2). Article no. 13. DOI: 10.1007/s40891-020-00196-0
23. Ahela, A.J. Assessment of Modulus of Subgrade Reaction of Stabilized Soils Using Light Weight Deflectometer. Master's Thesis. Department of Civil Engineering. University of Kerbala, 2017. 163 p.

Information about the authors:

Howaidah Al-Salamy,
E-mail: howidah.f@s.uokerbala.edu.iq

Mahdi Al-Naddaf, *PhD*
ORCID: https://orcid.org/0000-0002-6643-8449
E-mail: mahdi.a@uokerbala.edu.iq

Raid Almuhanna, *PhD*
E-mail: raidr@uokerbala.edu.iq

Received 15.02.2023. Approved after reviewing 29.08.2023. Accepted 29.03.2024.